The Astrophysical Journal, 986:49 (10pp), 2025 June 10 https://doi.org/10.3847/1538-4357/adceb6

Constraining the Mass of a Hypothetical Secondary Black Hole in M87 with the NANOGrav 15 yr Data Set

Motoki Kino[1,2], Masahiro Nagashima[3], Hyunwook Ro[4], Yuzhu Cui[5,6], Kazuhiro Hada[7,8], and Jongho Park[9,10]
[1] Kogakuin University of Technology & Engineering, Academic Support Center, 2665-1 Nakano-machi, Hachioji, Tokyo 192-0015, Japan; motoki.kino@gmail.com
[2] National Astronomical Observatory of Japan, 2-21-1 Osawa, Mitaka, Tokyo 181-8588, Japan
[3] Faculty of Education, Bunkyo University, 3337, Minami-ogishima, Koshigaya, Saitama 343-8511, Japan
[4] Korea Astronomy & Space Science Institute, Daedeokdae-ro 776, Yuseong-gu, Daejeon 34055, Republic of Korea
[5] Institute of Astrophysics, Central China Normal University, Wuhan 430079, People's Republic of China
[6] Research Center for Astronomical Computing, Zhejiang Lab, Hangzhou 311100, People's Republic of China
[7] Graduate School of Science, Nagoya City University, Yamanohata 1, Mizuho-cho, Mizuho-ku, Nagoya, 467-8501, Aichi, Japan
[8] Mizusawa VLBI Observatory, National Astronomical Observatory of Japan, 2-12 Hoshigaoka-cho, Mizusawa, Oshu, 023-0861, Iwate, Japan
[9] School of Space Research, Kyung Hee University, 1732, Deogyeong-daero, Giheung-gu, Yongin-si, Gyeonggi-do 17104, Republic of Korea
[10] Institute of Astronomy and Astrophysics, Academia Sinica, P.O. Box 23-141, Taipei 10617, Taiwan
Received 2025 March 7; revised 2025 April 13; accepted 2025 April 18; published 2025 June 5

Abstract

Galaxy mergers, each hosting a supermassive black hole (SMBH), are thought to form SMBH binaries. Motivated by recent observations from the East Asian Very Long Baseline Interferometry (VLBI) Network (EAVN) showing periodic behavior in the M87 jet, a precession of about 11 yr and a transverse oscillation of about 0.9 yr, we constrain the mass of a hypothetical secondary black hole orbiting the primary SMBH in M87. To constrain the mass ratio between the primary SMBH (M_1) and the secondary black hole (M_2) defined as $q \equiv M_2/M_1 \leqslant 1$, and the length of the semimajor axis of the binary system (a), we impose the following three constraints: (i) the lower limit of a, below which the SMBH binary is expected to merge; (ii) the strain amplitude of the gravitational-wave background at nanohertz frequencies shown in the NANOGrav 15 yr data set; and (iii) a finite length of the semimajor axis of M_1, which can induce periodic behavior in the jet. By combining these constraints, we obtain the allowed parameter space for q and a. If either of the EAVN-detected periods (T) corresponds to the binary's orbital period, the allowed range of q is $6.9 \times 10^{-3} \leqslant q \leqslant 4.2 \times 10^{-2}$ for $T \approx 11$ yr, and $3.7 \times 10^{-2} \leqslant q \leqslant 1$ for $T \approx 0.9$ yr. VLBI astrometric monitoring of the jet base of M87 is essential to explore the allowed parameter space for q and a.

Unified Astronomy Thesaurus concepts: Active galactic nuclei (16); Gravitational wave astronomy (675); Radio interferometry (1346); Supermassive black holes (1663); Very long baseline interferometry (1769)

1. Introduction

Growing observational evidence suggests that most massive galaxies contain supermassive black holes (SMBHs) at their centers (J. Kormendy & D. Richstone 1995; D. Richstone et al. 1998). In the standard model of hierarchical structure formation, frequent galaxy mergers are expected (e.g., J. P. Ostriker & M. A. Hausman 1977; C. Lacey & S. Cole 1993), which can lead to the formation of SMBH binaries (e.g., M. C. Begelman et al. 1980; M. Milosavljević & D. Merritt 2001). Multiple mechanisms are capable of shrinking the binary orbital separation through intermediate stage(s), solving the so-called final-parsec problem (e.g., M. Milosavljević & D. Merritt 2003a, for review). Possible scenarios would be: interaction of the binary with a gas disk (e.g., A. Gould & H.-W. Rix 2000; P. J. Armitage & P. Natarajan 2005), a massive perturber (e.g., F. G. Goicovic et al. 2017; M. Bonetti et al. 2018), and nonaxisymmetric stellar distributions that allow for a high interaction rate between stars and the binary (A. Gualandris et al. 2017). At the last stages of their orbital evolution, binaries produce nanohertz gravitational-wave (GW) emission, which can be detected by pulsar timing arrays (PTAs) that systematically monitor a large number of millisecond pulsars.

The NANOGrav 15 yr data set actually provides the evidence for the presence of a low-frequency gravitational-wave background (GWB; G. Agazie et al. 2023a). The inferred GWB amplitude and spectrum are broadly consistent with astrophysical expectations for a signal from a population of SMBH binaries, although more exotic cosmological and astrophysical sources cannot be excluded (G. Agazie et al. 2023b). Astrophysically motivated models of SMBH binary populations can reproduce both the amplitude and shape of the observed low-frequency gravitational-wave spectrum.

Despite strong theoretical and observational support for the pairing of SMBHs following galaxy mergers, definitive evidence for the existence of close-separation SMBH binaries approaching merger remains elusive. Therefore, the next crucial step should be a focused search for these SMBH binaries. The GWB is expected to be strongly influenced by SMBH binaries at low redshift (J. S. B. Wyithe & A. Loeb 2003; M. Enoki et al. 2004; A. Sesana et al. 2004). In the nanohertz range, the GWB is primarily contributed by the population of low-redshift massive SMBH binaries with masses $>10^9\,M_\odot$ (e.g., see Figure 3 in M. Enoki et al. 2004). Hence, systematically narrowing the allowed mass range for companion black holes in massive SMBHs at low redshift is highly significant. This study aims to take the first step toward this goal. In this context, it is intriguing to investigate the presence or absence of a secondary black hole in M87, one of the most massive SMBHs in nearby galaxies (Event Horizon Telescope Collaboration 2019a; Event Horizon Telescope Collaboration et al. 2024; K. Hada et al. 2024). It has

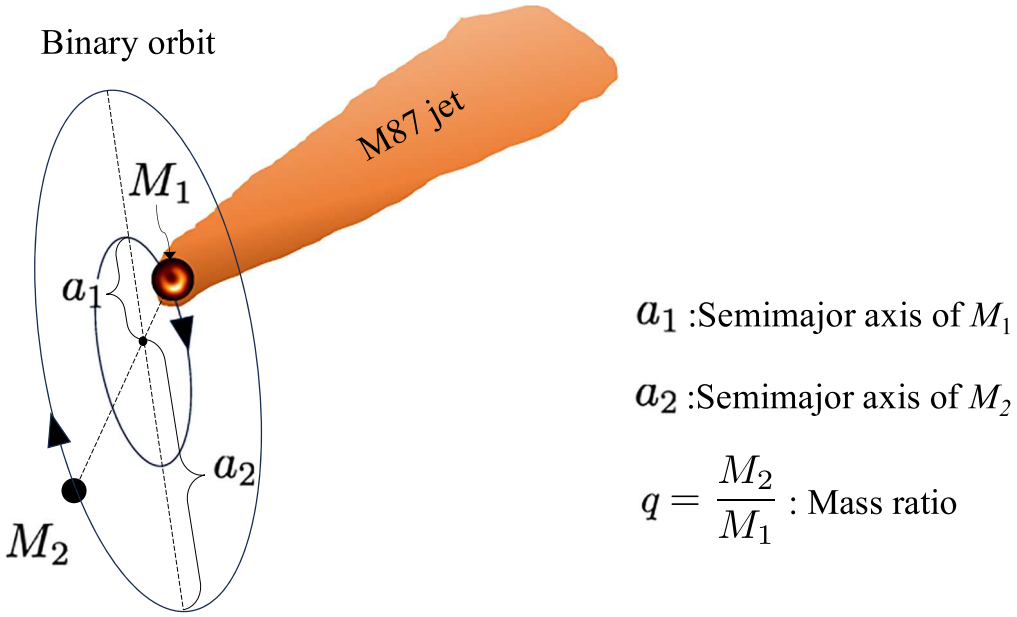

Figure 1. An illustration of the basic geometry of the hypothetical SMBH binary system considered in this study, with M87 used as a prime example. The primary black hole (M_1) generates the prominent radio jet observed at low frequencies, with the jet base anchored to M_1, while the secondary black hole (M_2) does not produce a jet. The reflex motion of M_1 likely induces periodic behaviors in the jet, such as precessing motion, transverse oscillation, and other similar effects (e.g., S. M. Ressler et al. 2024, and references therein). The M87 photo embedded in M_1 is adopted from Event Horizon Telescope Collaboration et al. (2024).

been reported that the luminous center of M87 and its active galactic nucleus are offset, suggesting that the SMBH may not be located at the galaxy's center of mass (D. Batcheldor et al. 2010). This displacement could be due to residual gravitational recoil oscillations following a merger event (D. Lena et al. 2014).

Interestingly, recent monitoring of the M87 jet using the East Asian Very Long Baseline Interferometry (VLBI) Network (EAVN) at 22 and 43 GHz has revealed the presence of periodic features (Y. Cui et al. 2023; H. Ro et al. 2023). The presence of periodicities is one of the most direct indicators of the orbital motion of an SMBH pair (e.g., M. C. Begelman et al. 1980; D. J. D'Orazio & A. Loeb 2018), suggesting that they may be linked to the orbital dynamics of an SMBH binary system. If M87 indeed hosts an SMBH binary system, the orbital period of the binary is expected to manifest in the periodic features detected in the M87 jet. Our ultimate aim is to identify sources of GWB detected by the NANOGrav. To this end, the immediate objective of the present work is to investigate the possible range of the mass ratio q and the semimajor axis a for the hypothetical SMBH in M87, the closest and most suitable example.

In Section 2, we briefly overview the model of binary orbital evolution following S.-S. Zhao et al. (2024). In Section 3, we summarize observational constraints for M87 that help constrain the allowed parameter space for q and a. In Section 4, we present the obtained constraints on q for M87. In Section 5, we discuss implications from the results. In Section 6, we summarize our findings.

2. SMBH Binary System

2.1. Basic Quantities of SMBH Binary

Throughout this work, we assume an SMBH binary system in a circular orbit for simplicity. The binary's total mass (M), semimajor axis (a), and the mass ratio (q) of the primary SMBH (M_1) and secondary SMBH (M_2) are defined by

$$M \equiv M_1 + M_2, \quad a \equiv a_1 + a_2 = \frac{1+q}{q} a_1, \quad q \equiv \frac{M_2}{M_1} \quad (0 < q \leqslant 1), \tag{1}$$

where a_1 and a_2 are the semimajor axis of the orbit of the primary and secondary SMBH, respectively (see Figure 1). When $q = 1$, $a = 2a_1$ holds. The angular velocity of the circular orbital motion (ω) is given by $\omega^2 = GM/a^3$. Therefore, the orbital period of the SMBH binary (T) and the angular scale of the semimajor axis on the sky (θ) are estimated as

$$T = \frac{2\pi}{\omega} = 17.6 \left(\frac{a}{10^{17}\,\mathrm{cm}}\right)^{3/2} \left(\frac{M}{10^9\,M_\odot}\right)^{-1/2} \mathrm{yr}, \tag{2}$$

and

$$\theta \equiv \theta_1 + \theta_2 = 67 \left(\frac{a}{10^{17}\,\mathrm{cm}}\right)\left(\frac{D}{100\,\mathrm{Mpc}}\right) \mu as, \tag{3}$$

where $\theta_1 = a_1/D$, $\theta_2 = a_2/D$, and D is the source distance from the Earth. This angular scale is well achievable by VLBI astrometric observations (e.g., M. J. Rioja & R. Dodson 2020, for review).

2.2. Binary Orbital Evolution

We provide a brief overview of a model describing the orbital evolution (shrinkage) of SMBH system following the previous works (e.g., M. C. Begelman et al. 1980; D. J. D'Orazio & A. Loeb 2018; S.-S. Zhao et al. 2024).

On kiloparsec scales, dynamical friction is known to be the primary mechanism for angular momentum loss (S. Chandrasekhar 1943). As the separation a decreases, dynamical friction becomes less effective, and individual interactions between each star and the binary system should be more effective. The timescale of the hardening can be given by

$t_{\rm hard} = 4\pi r_{\rm core}^2/(9C\sigma_\star a)$ where $r_{\rm core}$, C, and $\sigma_\star$ are the core radius, the hardening rate coefficient, and the stellar velocity dispersion of the host galaxy, respectively (G. D. Quinlan 1996; S.-S. Zhao et al. 2024). To be a binary system, the separation should be shorter than the hardening radius $a_{\rm hard}$, as the boundary between the dynamical friction process and the hardening state, which is given by

$$a_{\rm hard} = \frac{GM_1}{3\sigma_\star^2}. \tag{4}$$

The binary system is formed when a decreases to the range of $a \leqslant a_{\rm hard}$ (M. C. Begelman et al. 1980).

In a gas-driven case, the simple assumption is that the binary orbit shrinks via interaction with the environment, either by gas accretion or by application of positive torque to a circumbinary disk (e..g, R. R. Rafikov 2016). This process is highly uncertain (e.g., R. Miranda et al. 2017; Y. Tang et al. 2017; D. J. D'Orazio & A. Loeb 2018). Following S.-S. Zhao et al. (2024), here we set the gas-driven orbital decay timescale ($t_{\rm gas}$)

$$t_{\rm gas} = \frac{q}{(1+q)^2}\frac{1}{\dot{m}}t_{\rm Edd}, \quad \dot{m} \equiv \frac{\dot{M}}{\dot{M}_{\rm Edd}}, \tag{5}$$

where $\dot{m}$ is the mass accretion rate ($\dot{M}$) normalized by Eddington accretion rate ($\dot{M}_{\rm Edd}$), and the Eddington time, $t_{\rm Edd} \equiv M/\dot{M}_{\rm Edd} \approx 4.5 \times 10^7$ yr, is the time it takes for surrounding gas to accumulate until its total mass reaches the total mass of the binary system (i.e., M) at the Eddington accretion rate with the accretion efficiency of 10% (D. J. D'Orazio & A. Loeb 2018). From the relation of $t_{\rm hard} = t_{\rm gas}$, one can obtain $a_{\rm gas} = \frac{16\pi r_{\rm core}^2 \dot{m}}{9Ct_{\rm Edd}\sigma_\star}\frac{(1+q)^2}{4q}$.[11] When the separation decreases to $a_{\rm gas}$, there are no stars in the region, and gaseous environment plays the key role in the orbital evolution.

When the separation further decreases to $a_{\rm GW}$, the binary system begins to lose its angular momentum via GW emission. The timescale for GW radiation is given by

$$t_{\rm GW} = \frac{5}{64}\frac{c^5 a^4}{G^3 M^3}\left[\frac{4q}{(1+q)^2}\right]^{-1}, \tag{6}$$

by P. C. Peters (1964). This approximation is adequate for this work, since post-Newtonian corrections do not become appreciable until the final day scale of the merger (e.g., B. Kocsis et al. 2008). A criterion for GWs becoming important for binary evolution can be estimated as $t_{\rm GW}$ becomes shorter than the age of the Universe $t_{\rm Univ} \approx 1.38 \times 10^{10}$ yr (e.g., D. J. D'Orazio & M. Charisi 2023, for review). For M87, this happens where $a \sim 10^{18}$ cm (see Section 4 for details).

3. Observational Constraints for M87

In preparation for applying the aforementioned SMBH binary model to M87, we summarize relevant observational constraints for M87. Hereafter, we assume that that the black hole shadow observed by the Event Horizon Telescope (EHT) corresponds to the primary SMBH. We denote the EHT-constrained black hole mass as $M_{\rm EHT} \equiv (6.5 \pm 0.7) \times 10^9\, M_\odot$ (Event Horizon Telescope Collaboration 2019a, 2019b, 2019c, 2019d, 2019e, 2019f) and adopt this as the mass of the primary SMBH, $M_1 = M_{\rm EHT}$. The gravitational radius of the primary SMBH is denoted by r_g. This corresponds to the angular scale of gravitational radius $\theta_g \equiv GM_{\rm EHT}/c^2D = 3.8 \pm 0.4\,\mu as$ at the distance of $D = 16.8$ Mpc (J. P. Blakeslee et al. 2009; Event Horizon Telescope Collaboration 2019f).

3.1. Periodic Behaviors of the Jet

As mentioned in Section 1, the recent monitoring program of the M87 jet using EAVN at 22 and 43 GHz has detected periodic behaviors in the jet (Y. Cui et al. 2023; H. Ro et al. 2023). Y. Cui et al. (2023) investigated the time sequence of 170 VLBI images of the M87 jet obtained by the EAVN and other VLBI observations between 2000 and 2022. It is found that the position angle of the jet direction near the core changes with the precession period of

$$T_{\rm prec} = 11.24 \pm 0.47 \text{ years}. \tag{7}$$

H. Ro et al. (2023) monitored the M87 jet at KVN and VERA Array (KaVA) 22 GHz from 2013 December to 2016 June with the average time interval of 0.1 yr, and they found that the ridge lines show transverse oscillations with a period of

$$T_{\rm trans} = 0.94 \pm 0.12 \text{ years}. \tag{8}$$

The reflex motion of the primary SMBH M_1 could induce oscillatory motion in the radio jet. For convenience, we define the semimajor axis a_T corresponding to a binary orbital period T, given by

$$a_T \equiv \left(\frac{GMT^2}{4\pi^2}\right)^{1/3} = \left(\frac{GM_1T^2}{4\pi^2}\right)^{1/3}(1+q)^{1/3}, \tag{9}$$

which is essentially the same as Equation (2).

3.2. Tentative Constraints on a_1 by VLBI Astrometry

The presence of a secondary SMBH induces reflex motion of the primary SMBH, M_1, around the center of mass with the radius of a_1 (see Figure 1). Although constraining a_1 is challenging, VLBI phase-referencing observations can provide upper limits on a_1. K. Hada et al. (2012) provided a unique comparison of two epochs of data. The core position remained stable on $\sim 30\,\mu$as (equivalent to $\sim 8\,r_g$) as on the projected scale on the sky during the 10 days. A similar result was reported during the very high energy (VHE) flare in 2008 that remained stable within $\sim 45\,\mu$as (equivalent to $\sim 12\,r_g$; V. A. Acciari et al. 2009). These studies tentatively place an upper limit of a_1. However, it should be noted that the constraints on a_1 derived from previous VLBI astrometric observations have significant limitations. The primary limitation is the short monitoring duration, which makes it difficult to investigate binary systems with long orbital periods. We will discuss this issue in more detail in the next section.

3.3. The NANOGrav 15 yr Data Set

Following K. Schutz & C.-P. Ma (2016), one can place constraints on a secondary black hole using the GWB strain amplitude obtained by PTA observations. The amplitude of continuous GWs can be parameterized by the dimensionless characteristic strain amplitude h_c, averaged over the whole sky (e.g., F. A. Jenet et al. 2006). For an SMBH binary at leading post-Newtonian order under the assumption of circular orbits

[11] Note that this form neglects the loss-cone depletion for simplicity, which will not affect the following arguments (S.-S. Zhao et al. 2024).

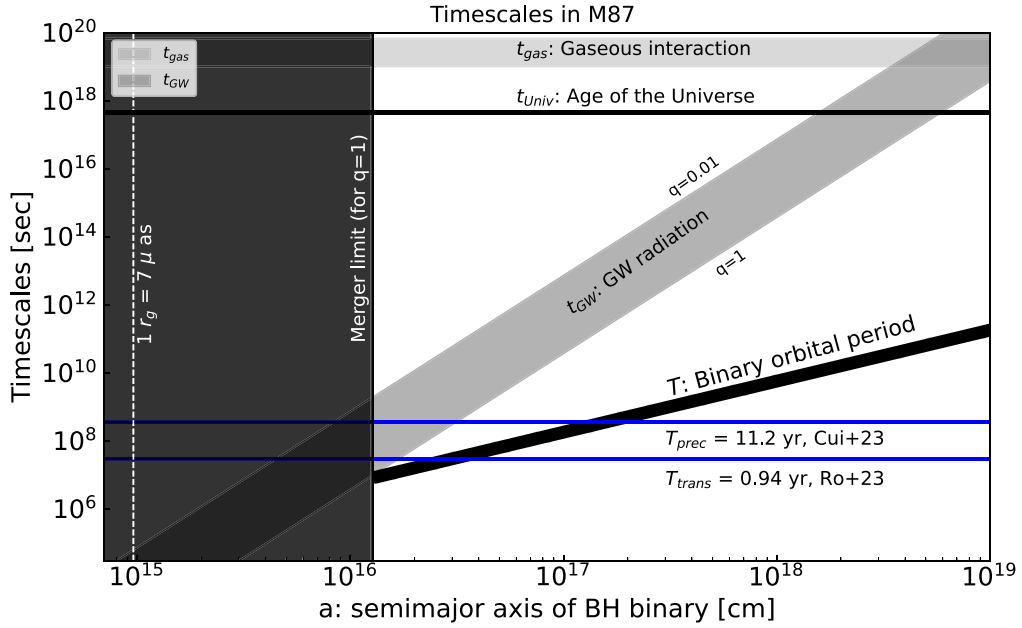

Figure 2. Comparison of characteristic timescales in M87. The binary orbital period ($T \propto a^{3/2}$), represented by the thick line, is the most important timescale, as given by Equation (2). The timescale for GW radiation, $t_{\rm GW} \propto q^{-1}a^4$, is represented by a dark-gray thick line for $0.01 \leqslant q \leqslant 1$. We also plot the two blue lines representing $T_{\rm prec}$ and $T_{\rm trans}$. When $T = T_{\rm prec}$, the corresponding semimajor axis is approximately $a \approx 1 \times 10^{17}$ cm. When $T = T_{\rm trans}$, the corresponding semimajor axis is approximately $a \approx 3 \times 10^{16}$ cm. When $t_{\rm GW} < T$, the SMBH binary will merge into a single SMBH. This occurs when the semimajor axis is less than approximately $a \lesssim 1 \times 10^{16}$ cm. In addition, $t_{\rm gas}$ for M87 is shown in light gray, and is even longer than $t_{\rm Univ}$ due to its small mass accretion rate of $\dot{m} \sim 10^{-6}$.

and evolution purely by energy loss via GW radiation, the strain amplitude is given by

$$h_c = 2.76 \times 10^{-14}\left(\frac{\mathcal{M}_{\rm ch}}{10^9\,M_\odot}\right)^{5/3} \times \left(\frac{D}{10\,{\rm Mpc}}\right)^{-1}\left(\frac{f_{\rm GW}}{10^{-8}\,{\rm Hz}}\right)^{2/3}, \quad (10)$$

and

$$f_{\rm GW} = 6.3 \times 10^{-9}\left(\frac{T}{10\,{\rm year}}\right)^{-1}\,{\rm Hz}, \quad (11)$$

where $f_{\rm GW} = 2/T$, and $\mathcal{M}_{\rm ch} = \left(\frac{M_1 M_2}{M}\right)^{3/5} M^{2/5}$, are the frequency of the emitted GWs, and the chirp mass of the binary, respectively (K. Schutz & C.-P. Ma 2016). The chirp mass is known to be rewritten as $\mathcal{M}_{\rm ch} = M_1 \frac{q^{3/5}}{(1+q)^{1/5}}$. Since $q \leqslant 1$, the chirp mass follows $\mathcal{M}_{\rm ch} = \frac{q^{3/5}}{1+q^{6/5}} M \leqslant 2^{-6/5} M \approx 0.435M$. The $\mathcal{M}_{\rm ch}$ is at a maximum for $q = 1$ and decreases monotonically as q decreases. The GWB strain amplitude constrained by the NANOGrav15 roughly indicates $h_{\rm GWB} \approx 1 \times 10^{-14}$ (see Figure 1 in G. Agazie et al. 2023b). To avoid the overproduction of the GWB as suggested by the NANOGrav15 data set, the condition $h_{\rm GWB} \geqslant h_c$ is satisfied. Then, one can obtain the lower limit $a_{\rm GWB}$ in the frequency range of $2\,{\rm nHz} \lesssim f_{\rm GW} \lesssim 30\,{\rm nHz}$ as follows:

$$a_{\rm GWB} = 1.4 \times 10^{17}\left(\frac{M_1}{10^9 M_\odot}\right)^2\left(\frac{D}{10\,{\rm Mpc}}\right)^{-1} \times \left(\frac{h_{\rm GWB}}{1 \times 10^{-14}}\right)^{-1} q\,{\rm cm}, \quad (12)$$

where the relations of $f_{\rm GW} = (GM/a_{\rm GWB}^3)^{1/2}/\pi$ and $\mathcal{M}_{\rm ch} = \frac{q^{3/5}}{1+q^{1/5}} M_1$ are used to obtain Equation (12). Thus, the NANOGrav 15 yr data set can place an upper limit through the GWB strain amplitude.

3.4. Persistent EHT Ring Images

As a decreases to subparsec scale, we must account for $t_{\rm GW} \propto a^4$, as $t_{\rm GW}$ becomes significantly short. If M87 were in a merger phase, the black hole shadow and its surrounding ring image of M87 would exhibit highly nonlinear and dynamic features (A. Yumoto et al. 2012; A. Bohn et al. 2015; P. V. P. Cunha et al. 2018). However, EHT observations clearly show the persistent ring image, at least in 2017 and 2018 (Event Horizon Telescope Collaboration 2019a; Event Horizon Telescope Collaboration et al. 2024), allowing us to readily exclude that the binary system is already in a merging phase.

When $t_{\rm GW}$ is shorter than the binary orbital period (T), the binary system is expected to merge into a single SMBH (see Figure 2). Based on this criterion, we define the timescale $t_{\rm merge}$, which satisfies $t_{\rm merge} \equiv t_{\rm GW}(a = a_{\rm merge})$. Using this definition, we find that $t_{\rm merge} \approx 0.3\,{\rm yr}$ ($q = 1$) at $a \approx 1.3 \times 10^{16}\,{\rm cm}$ for M87 (see Figure 2). The corresponding lower limit a below which the binary black holes are expected to merge into a single SMBH can be defined by

$$a_{\rm merge} = \left[\frac{256 G^3 M_1^3 t_{\rm merge}}{5c^5} q(1+q)\right]^{1/4}. \quad (13)$$

Due to the weak dependence of $a_{\rm merge}$ on $t_{\rm merge}$, i.e., $a_{\rm merge} \propto t_{\rm merge}^{1/4}$, the uncertainty in $t_{\rm merge}$ does not significantly impact the estimate of $a_{\rm merge}$.

4. Results

Here, we present the results of applying the SMBH binary model to M87. As illustrated in Figure 1, we consider the situation where M_1 generates the observed prominent radio jet in M87, while M_2 does not produce a jet.

4.1. Comparison of Timescales

Figure 2 presents a comparison of relevant timescales in M87. The orbital period (T) and the timescale of GW radiation ($t_{\rm GW}$) are given by Equations (2) and (6), respectively. To plot T and $t_{\rm GW}$, we set $0.01 \leqslant q \leqslant 1$. For plotting $t_{\rm gas}$, we set $q = 0.01$ and choose the mass accretion rate as $\dot{M} = (3 - 20)\times 10^{-4}\, M_\odot\ {\rm yr}^{-1}$, based on the result of Event Horizon Telescope Collaboration et al. (2021). Figure 2 shows that the range of semimajor axis where T is comparable to $T_{\rm prec}$ or $T_{\rm trans}$ lies within approximately $10^{16}\,{\rm cm} \lesssim a \lesssim 10^{17}\,{\rm cm}$, well-aligned with spatial resolutions of recent VLBI observations. This makes M87 the best candidate for starting a detailed study of a potential SMBH binary system. It is well known that a criterion that GWs become important for binary evolution can be estimated as $t_{\rm GW} \leqslant t_{\rm Univ} \approx 1.38 \times 10^{10}\,{\rm yr}$ (D. J. D'Orazio & M. Charisi 2023, for review). From Figure 2, one can see that this condition is met when $a \lesssim 10^{18}\,{\rm cm}$ for M87.[12]

Compared to $t_{\rm gas}$ discussed in this work and previous studies (D. J. D'Orazio & A. Loeb 2018; S.-S. Zhao et al. 2024), a notable difference is identified: $t_{\rm gas}$ appears excessively long in the case of M87. This is naturally understood, as both of the aforementioned prior studies (D. J. D'Orazio & A. Loeb 2018; S.-S. Zhao et al. 2024) considered a mass accretion rate of $\dot{m} \sim 1$, whereas M87, on the contrary, has the mass accretion rate on the order of $\dot{m} \sim 10^{-6}$, which is substantially smaller than $\dot{m} \sim 1$. Thus, at first glance, gaseous interactions appear negligible in the current state of M87. However, $t_{\rm gas}$ exceeds the age of the Universe $t_{\rm Univ} \approx 1.38 \times 10^{10}\,{\rm yr}$, raising the well-known "final-parsec problem,"—namely, how a binary system can form under such circumstance (e.g., M. Milosavljević & D. Merritt 2003b; D. J. D'Orazio & M. Charisi 2023, for review). One possibility may be the presence of a specific period, during which $\dot{m}$ becomes significantly elevated. Interactions and mergers between galaxies are known to trigger large-scale nuclear gas inflows, supplying gas to SMBHs (e.g., L. Hernquist 1989; T. Di Matteo et al. 2005; P. F. Hopkins et al. 2006, 2008). Such galaxy interaction or merger events could promote temporarily elevated $\dot{m}$ levels. Another possibility is the presence of cold gas. Recent Atacama Large Millimeter/submillimeter Array CO(1–0) observations reported by M. Ray & C.-Y. Hwang (2024) revealed the distribution of molecular clouds within approximately 100 pc of the M87 nucleus. This newly identified cold gas could potentially reduce $t_{\rm gas}$. Additionally, unequal-mass SMBH binaries are known to show significantly higher eccentricity than equal-mass SMBH binaries, which may accelerate the decrease in a (e.g., S. Mikkola & M. J. Valtonen 1992; M. Enoki & M. Nagashima 2007; T. Matsubayashi et al. 2007; M. Iwasawa et al. 2011). Since the primary aim of this paper is not to investigate the formation of a binary system in M87 in detail, but rather to constrain the allowed range of q based on the latest observational constraints, we do not undertake detailed modeling of $t_{\rm gas}$ in M87.

[12] A pioneering study by N. Yonemaru et al. (2016) investigated GW emission from M87. However, their analysis considered a larger a compared to the present work.

4.2. Allowed Parameter Space for q and a

In Figure 3, we present the allowed parameter space for q and a in M87. All of the gray-shaded regions represent the excluded areas for q and a, while the remaining white region is the allowed parameter space for q and a. As we consider the SMBH binary system, the upper limit of a is inherently constrained by the condition of $a \geqslant a_{\rm hard} \approx 5\times 10^{19}(M_1/10^9 M_\odot)$cm, assuming $\sigma_\star \approx 300\,{\rm km\,s^{-1}}$.

4.2.1. The Cases of T = T$_{prec}$ and T = T$_{trans}$

Here, we consider the cases of $T = T_{\rm prec}$ and $T = T_{\rm trans}$. To constrain q and a, we impose the following three constraints:

1. The lower limit of a is constrained by the condition of $a > a_{\rm merge}$. When the semimajor axis contracts to $a \leqslant a_{\rm merge}$, as given by Equation (13), the SMBH binary undergoes a merger due to the loss of angular momentum and energy through GW radiation. The black region below the "merger limit" corresponds to this case. The entire range for $T = T_{\rm prec}$ or $T = T_{\rm trans}$ remains unaffected by this "merger limit."
2. The region excluded by the NANOGrav15 observation is shaded in dark gray. To avoid the overproduction of the GWB, as suggested by the NANOGrav15 data set, the condition $a \geqslant a_{\rm GWB}$ is imposed at the frequency range $2\,{\rm nHz} \lesssim f_{\rm GW} \lesssim 30\,{\rm nHz}$. As mentioned in Section 3.3, here we set $h_{\rm GWB} = 1 \times 10^{-14}$ based on G. Agazie et al. (2023a). From Figure 3, we find that the upper limit of the allowed range is bounded by the NANOGrav 15 yr limit in the case of $T = T_{\rm prec} = 11.2\,{\rm yr}$. In contrast, the case of $T = T_{\rm trans} = 0.94\,{\rm yr}$ is not excluded by the NANOGrav 15 yr limit because the frequency range covered by the NANOGrav does not extend beyond $f_{\rm GW} \approx 30\,{\rm nHz}$.
3. A lower limit of a_1 is set here. As illustrated in Figure 1, the reflex motion of M_1 induces periodic behavior in the jet for both $T = T_{\rm prec}$ and $T = T_{\rm trans}$. Consequently, a_1 cannot be zero and must have a finite value. Since the jet behavior at different a_1 values is not well investigated, we assume a lower limit of $a_1 = 1\, r_g$, labeled as a (for $a_1 = r_g$). Below this threshold, the jet is unlikely to exhibit a distinct periodic signature.

By combining all of the constraints described above, we obtain the allowed range of q as follows:

$$6.9 \times 10^{-3} \leqslant q \leqslant 4.2 \times 10^{-2} \times ({\rm for}\ T = T_{\rm prec} = 11.2\ {\rm yr}), \quad (14)$$

$$3.7 \times 10^{-2} \leqslant q \leqslant 1 \quad ({\rm for}\ T = T_{\rm trans} = 0.94\ {\rm yr}). \quad (15)$$

The blue lines in Figure 3 represent the allowed ranges for these cases. The intersection points of the excluded regions and a_T are marked by the star-shaped dot to facilitate visual identification of the allowed parameter ranges.

4.2.2. The Case of neither T = T$_{prec}$ nor T = T$_{trans}$

Next, we consider the Case of neither $T = T_{\rm prec}$ nor $T = T_{\rm trans}$. In this case, the entire white region in Figure 3 is the allowed parameter space for q and a, resulting in a significant expansion of the allowed parameter space. The origin of the observed jet precession (Y. Cui et al. 2023) and the transverse oscillation (H. Ro et al. 2023) should not be a

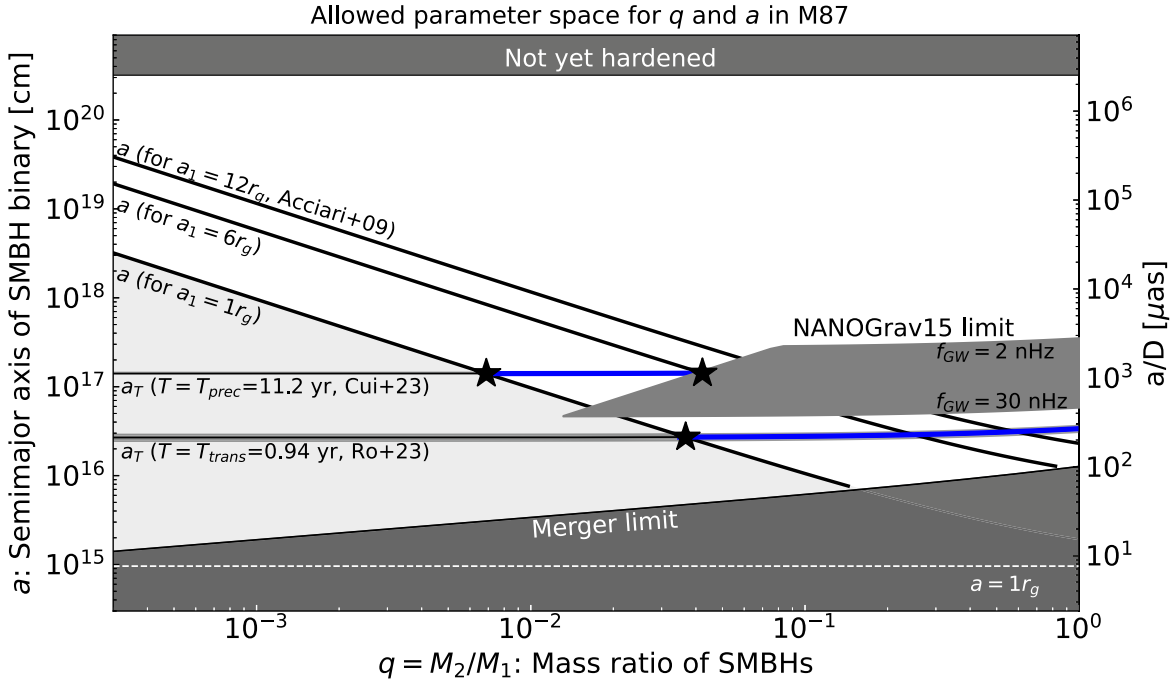

Figure 3. Allowed parameter space for q and a in M87. All of the gray-shaded regions represent the excluded areas for q and a, while the remaining white region is the allowed parameter space for q and a. In particular, the allowed ranges for the cases of $T = T_{\rm prec}$ are $T = T_{\rm trans}$ are shown with blue lines. The upper limit of a is constrained by the condition of $a < a_{\rm hard}$. The lower limit of a is constrained by the condition of $a > a_{\rm merge}$. The upper limit of q is partially constrained by the GWB strain amplitude obtained by the NANOGrav15 (G. Agazie et al. 2023a). This constraint applies only to the range of 2 nHz $\lesssim f_{\rm GW} \lesssim$ 30 nHz. The lower limit of a_1 is determined by the existence of a reflex motion of M_1, shown as the light-gray-shaded region, where $a_1 > 1\ r_g$ is assumed. In the cases of $T = T_{\rm prec}$ and $T = T_{\rm trans}$, the lower limit of q is determined by $T(a_1 = 1\ r_g) = T_{\rm prec}$ or $T(a_1 = 1\ r_g) = T_{\rm trans}$ and is marked as stars. The upper limit of q is bounded by the NANOGrav 15 limit in the case of $T = T_{\rm prec}$.

reflex motion in the SMBH binary. Instead, it should be naturally attributed as suggested in each respective paper.

Although the merger limit and the NANOGrav15 limit offer important limits on the allowed parameter space, it is intriguing to identify a gap-window region in between them where the case $q \sim 1$ remains valid. Coincidentally, the gap-window region envelopes the aforementioned case of $T = T_{\rm trans}$. Similar to the case mentioned above, the gap-window region with $q \sim 1$ aligns with the case of approximately $a_1 \sim 10\ r_g$. Proposed approaches for investigating the allowed parameter space will be also discussed in Section 5.

Additionally, it is worth noting that a previous work by M. Safarzadeh et al. (2019) also addressed q in M87. However, a key difference between their study and the present work lies in the GW frequency range to which the PTA limit is applied. The upper limit of $a_{\rm T}$, which is approximately 0.01 pc in the PTA limit adopted in M. Safarzadeh et al. (2019; the black hatched area in Figure 1 of their paper), corresponds to the GW frequency range of $f_{\rm GW} \gtrsim 50$ nHz, based on Equations (9) and (11). However, the effective frequency range of NanoGrav 15 yr data set is 2 nHz $\lesssim f_{\rm GW} \lesssim$ 30 nHz (G. Agazie et al. 2023a). This difference in the GW frequency range likely explains why the gap-window region found in this work does not appear in M. Safarzadeh et al. (2019).

5. Discussion

5.1. Astrometric Observations with Current VLBI Facilities

It is widely recognized that VLBI astrometric observations, through the direct tracking of orbital motions, could provide conclusive evidence of subparsec separation SMBH binaries on orbital timescales (e.g., D. J. D'Orazio & M. Charisi 2023, for review).[13] However, one significant limitation of VLBI astrometry is the requirement for expensive, multiepoch VLBI observations, restricting its feasibility to a limited number of targets. Therefore, we initiate an investigation of M87 as a likely target system, given the periodic behavior observed in its jet.[14] Below, we briefly discuss strategies for conducting VLBI astrometric observations using current VLBI facilities.

Our ultimate science goal is to identify definitive evidence for the existence of close-separation SMBH binaries nearing mergers. Therefore, cases with larger q would be more intriguing than those with smaller q. In this context, the gap-window region between the NANOGrav15 limit and the merger limit appeared in Figure 3 is of great interest for investigation through VLBI astrometric observations. The upper limit of the gap-window region is defined by the upper bound of the NANOGrav's frequency range, $f_{\rm GW} = 30$ nHz, which corresponds to a binary orbital period of $T \approx 2$ yr. To investigate the presence of reflex motion in the gap-window region, it is crucial to detect at least one full cycle of periodic motion or a slightly longer duration. This corresponds to approximately 2–3 yr. As a first step, it would be reasonable to begin exploration in the gap-window region around approximately $\sim$40 μas ($a_1 \approx 6\ r_g$), comparable to previous works, rather than attempting to address the scale of $\sim$4 μas ($a_1 \approx 1\ r_g$) from the beginning. The position error ($\Delta\theta$)

[13] Astrometric monitoring observations in the near-infrared band, aimed at determining SMBH binaries, are also discussed by J. Dexter et al. (2020).

[14] In contrast to M87, OJ287 ($z = 0.306$) is a well-discussed SMBH binary candidate due to its repeated double-peaked outburst features in the optical band with 12 yr intervals and complex transverse motion of its jet (e.g., A. Sillanpaa et al. 1988; S. Britzen et al. 2018; S. Britzen et al. 2023). Recently, X. Cheng et al. (2023) discussed a feasibility for future VLBI astrometry, emphasizing the importance of a suitable reference source.

originated from the phase error ($\Delta\phi$) is generally expressed as follows:

$$\Delta\theta = \frac{\lambda_{\rm obs}}{2\pi D_{\rm bl}}\Delta\phi \approx c\Delta\tau_0 \sec Z \tan Z \Delta Z \quad (16)$$

where $D_{\rm bl}$, $\lambda_{\rm obs}$, $\Delta\tau_0$, and Z, are the baseline length, the observing wavelength, the residual vertical delay, and the local source zenith angle, respectively (M. J. Reid et al. 1999; A. R. Thompson et al. 2001). For instance, it can be estimated as $\Delta\theta \sim 28\ \mu$as at 43 GHz (7 mm) for the tropospheric zenith delays within $\Delta\tau_0 \approx 2$ cm accuracy for the VERA array (M. Honma et al. 2008), $\Delta Z = 0.^{\circ}5$, $Z = 50^{\circ}$, and $D_{\rm bl} \approx 2 \times 10^3$ km (e.g., S. Koyama et al. 2015; K. Niinuma et al. 2015). While VLBI astrometry observations can directly constrain a_1, only a limited number of such observations have been conducted for M87 in the past (V. A. Acciari et al. 2009; K. Hada et al. 2012, 2014). Figures 2 and 3 clearly indicate that VLBI astrometric monitoring of M87's jet base over just a few months is insufficient. Long-term monitoring would be essential to better constrain the allowed ranges for a and q. Given the practical challenges of conducting continuous VLBI astrometry observations over a 10 yr period, we propose a more feasible approach: initiating a 1–2 yr VLBI astrometry pilot study of M87 to obtain initial results. If the pilot data indicate a systematic motion of a_1, it would motivate the continuation of longer-term observations.

One potential caveat would be the overlapping of newly ejected blob component(s) onto the underlying continuous jet image during flaring events. K. Hada et al. (2014) conducted VERA astrometry for the M87 core with respect to the core position of M84, during the VHE flaring event in 2012. They detected core shifts between 22 and 43 GHz, with a mean value of $(\Delta x_{22-43}, \Delta y_{22-43}) = (64, 95)\ \mu$as. The radio core flux densities showed frequency-dependent evolution, with more rapid increases at higher frequencies and greater amplitude variations. The light curves revealed a time lag between the peaks at 22 and 43 GHz, constrained to approximately 35–124 days. This suggests that a newly born radio-emitting component was generated near the black hole during the VHE flaring event in 2012 and subsequently propagated outward with the speed of $\sim(0.04$–$0.22)\,c$. Such a propagation of the new component may introduce errors in estimating the location of M_1. However, since the duration of the VHE flaring event is limited to less than a month (K. Hada et al. 2024), and the newly born radio-emitting component can be identified through VLBI observations (K. Hada et al. 2014), it may be possible to minimize errors in estimating the location of M_1 caused by the flare-associated component.

Another caveat could be an annual parallax when exploring $T \approx 1$ yr. Annual parallax is geodetic effects related to Earth's orbital motion around the Sun. It is based on the principle of triangulation. This shift is caused by the change in perspective as Earth moves from one side of its orbit to the other, creating a slight change in the angle from which we view a target source. Therefore, if $T = T_{\rm trans} \approx 1$ yr is the case, then one must carefully discriminate the reflex motion to the annual parallax (H. Sudou et al. 2003). With the definition $1'' \equiv 1$ au$/1$ pc, the expected amplitude of the annual parallax for $D = 16.8$ Mpc corresponds to 0.06 μas, which is significantly smaller than the target accuracy of this work. Moreover, long-period observations will help overcome challenges in exploring $T \approx 1$ yr. If astrometric observations are continuously conducted over a long period of 10 yr, assuming this is practically feasible, the binary is expected to complete 9.4 orbits, which should be distinguishable from completing 10 orbits.

Multifrequency receivers designed for VLBI astrometry are currently being installed or scheduled to be installed on many VLBI telescopes worldwide (R. Dodson et al. 2023, for review). In the near future, multifrequency VLBI systems will significantly advance our ability to address key scientific questions. In particular, phase-referencing observations at 86 GHz, utilizing the frequency phase transfer technique (M. J. Rioja & R. Dodson 2020; R. Dodson et al. 2023; S. Issaoun et al. 2023), will enable us to perform phase-referencing observations illustrated in Figure 1. This is because 86 GHz imaging can reveal the ring-like accretion structure image at the M87 jet base (R.-S. Lu et al. 2023; J.-S. Kim et al. 2025), facilitating more accurate tracking of M_1, which is likely located within this structure. However, a major confounding effect in extracting potential orbital motion is expected to arise from structural variations in the jet base region, such as an ejection of a new jet component and/or jet–disk interactions. Future projects of the next-generation Event Horizon Telescope (ngEHT; S. S. Doeleman et al. 2023; M. D. Johnson et al. 2023) and the black hole Explorer (BHEX; M. D. Johnson et al. 2024), will be capable of capturing detailed structural changes in the jet base region. Since such structural variations may complicate the extraction of pure orbital motion of M_1, ngEHT and BHEX will play a crucial role in mitigating the confounding effect.

5.2. Future Astrometric Observations with NgVLA

J. M. Wrobel & T. J. W. Lazio (2022) highlighted that the next-generation Very Large Array (ngVLA; E. J. Murphy et al. 2018) will be a powerful tool for astrometric observations of SMBH binary candidates. They noted that using multiple phase calibrators, separated from a target source by $<1^{\circ}$–2° for the phase-referencing observation, would allow one to achieve position accuracy levels on the order of 1 μas at millimeter wavelengths (see also M. J. Rioja & R. Dodson 2020). From Figure 3, it is clear that position accuracy levels on the order of 1 μas correspond to the region below the "merger limit" in the case of M87. Therefore, ngVLA astrometric observations may be unnecessarily precise for M87 when searching for a hypothetical secondary black hole. However, it is worth identifying intriguing scientific cases with future ngVLA observations.

We emphasize that the below-merger-limit domain corresponds to the case where M87 has a single black hole. Therefore, this domain offers a valuable opportunity to avoid the potential overlap of multiple origins for any positional shifts of M_1 that future ngVLA astrometric observations might detect. In this context, we discuss the feasibility of searching for fuzzy dark matter (FDM) at the center of M87. An SMBH at the center of a star cluster or galaxy experiences Brownian motion due to gravitational encounters with stars, leading to displacement from its central position (e.g., J. N. Bahcall & R. A. Wolf 1976; D. Merritt et al. 2007). The nuclear point (SMBH location) of M87 appears to be offset from the galaxy's photocenter by about 6 pc (D. Batcheldor et al. 2010). This off-center displacement can be attributed to gravitational interactions with stars over 10^{10} s (P. Di Cintio et al. 2020).

The expected speed of this gravitational Brownian motion due to stars $\sigma_{\rm BH/\star}$ can be approximately estimated as

$$\sigma_{\rm BH/\star} \approx \left(\frac{m_\star}{M}\right)^{1/2}\sigma_\star \approx 0.001\ {\rm km\ s^{-1}}\left(\frac{\sigma_\star}{100\ {\rm km\ s^{-1}}}\right), \quad (17)$$

where $m_\star$ and $\sigma_\star$ are the mass of a typical star, and the stellar velocity dispersion, respectively (M. J. Reid & A. Brunthaler 2004; D. Merritt et al. 2007)[15] and Equation (17) is the case for $m_\star/M \approx 10^{-10}$. However, gravitational Brownian motion is not only caused by stars but also by the surrounding dark matter. It generally reflects the physical properties of the entire surrounding environment. One of the interesting explorations for the surrounding environment could be constraining the mass of dark matter via gravitational Browninan motion of SMBHs in a dark matter halo. FDM, consisting of ultralight axions, has been proposed to mitigate galactic-scale problems within the cold dark matter scenario (e.g., E. G. M. Ferreira 2021, for review). A. A. El-Zant et al. (2020) assumed that the SMBH achieves equilibrium with the fluctuations; that is, there is a balance between the effects of fluctuation and dissipation, the latter being due to dynamical friction.[16] Assuming the energy equi-partition condition, the velocity dispersion of the SMBH caused by the FDM ($\sigma_{\rm BH/FDM}$) is related to the FDM velocity dispersion ($\sigma_{\rm halo}$) as $M\sigma^2_{\rm BH/FDM} = m_{\rm eff}\,\sigma^2_{\rm halo}/2$ where $m_{\rm eff}$ denotes the effective mass of FDM quasi-particles. Then, the velocity dispersion of the SMBH caused by the FDM is given by

$$\sigma_{\rm BH/FDM} \approx \left(\frac{m_{\rm eff}}{M}\right)^{1/2}\sigma_{\rm halo} \approx 25\ {\rm km\ s^{-1}} \times\left(\frac{m_{\rm ax}c^2}{10^{-22}\ {\rm eV}}\right)^{-1/2}\left(\frac{M}{6\times10^9\,M_\odot}\right)^{-1/6} f(x)^{1/2}, \quad (18)$$

where $f(x) = (1+x^2/3)(x^2+3)^2/[(1+x^2)(x^2+2)]^2$, $x = r/r_{\rm core}$, and $m_{\rm ax}$ is the axion mass (see details A. A. El-Zant et al. 2020). Interestingly, $\sigma_{\rm BH/FDM} \gg \sigma_{\rm BH/\star}$ is expected. The corresponding angular velocity of SMBH Brownian motion, however, is $<1\,\mu{\rm as\,yr^{-1}}$. Another difficulty may be an existence of secular proper motion. As pointed out by J. M. Wrobel & T. J. W. Lazio (2022), there could be relative motion even between M87 and a reference source. M87 is located at the center of the Virgo cluster, and reference sources commonly used for astrometric observations of M87 (e.g., M84) are also sufficiently within the virial radius of the Virgo cluster (about 10^3 kpc; A. Simionescu et al. 2017) and reach virial equilibrium. Recently, the infalling velocity M49 group located outside the virial radius of the Virgo cluster, has been estimated as $v_{\rm infall} \approx 300$–$640\,{\rm km\,s^{-1}}$ by Y. Su et al. (2019), corresponding to $\dot\theta_{\rm infall} \approx 4 - 8\ \mu$ as yr^{-1}. The $\dot\theta_{\rm infall}$ would be superposed onto the possible gravitational Brownian motion of SMBH by FDM. Therefore, detecting $\sigma_{\rm BH/FDM}$ may not be straightforward. To achieve high-precision astrometry with $\dot\theta < 1\ \mu$ as yr^{-1}, astrometric observations at 86 GHz or higher would be required (e.g., S. Issaoun et al. 2023; W. Jiang et al. 2023; S.-S. Zhao et al. 2024).

5.3. Toward Localization of GWB Sources

R. W. Hellings & G. S. Downs (1983) highlighted that the angular correlation pattern for pulsar pairs averaged over the whole sky domain can serve an evidence of GWs, as the resulting correlation curve reflects a quadrupole nature of GWs (e.g., M. Maggiore 2018). However, the whole-sky average makes the Hellings–Downs curve insensitive to any particular direction of the sky. To overcome this problem, T. Sasaki et al. (2024) explored what happens in the pulsar correlation if the averaging domain is changed from the whole sky. They found that the angular correlation pattern for pulsar pairs within a chosen sky hemisphere has a dependence on a single GW compact source. They indicated that if a single GW source is dominant, the variation in a hemisphere-averaged angular correlation curve is the greatest when the chosen hemisphere has its north pole at the sky location of the GW source. According to T. Sasaki et al. (2024), a nearby GW source can be marginally detected when the distance (D) to the GW source is

$$D \lesssim 2\times10^2\ {\rm Mpc}\left(\frac{N_{\rm pulsar}}{10^2}\right)^{1/2}\left(\frac{\Delta\Gamma_{\rm H}}{0.1}\right)^{1/2} \times\left(\frac{\Delta t_a}{1\ \mu\ {\rm sec}}\right)\left(\frac{M}{6.5\times10^9 M_\odot}\right)^{5/3}\left(\frac{f_{\rm GW}}{1{\rm yr}^{-1}}\right)^{1/3}, \quad (19)$$

where $N_{\rm pulsar}$, $\Gamma_{\rm H}$, $\Delta\Gamma_{\rm H}$, and Δt_a are the total number of the observed pulsars in PTAs, the difference between the maximum and minimum of the hemisphere-averaged cross-correlation of pulsar pairs ($\Gamma_{\rm H}$), the variation of $\Gamma_{\rm H}$ for changing the inclination angle of the hemisphere from the GW source direction, and the delay in the measured pulse arrival time from the ath pulsar relative to the expected arrival time in the absence of gravitational waves, respectively. From this, it is clear that the distance of M87, $D = 16.8$ Mpc, falls well within the target range of this hemisphere-averaged method.

Enhancing PTA sensitivities is an important factor in relation to searching for GWB sources. There are, widely discussed, two ways to realize it. The first one is constructing the Square Kilometer Array (SKA). The SKA would significantly improve the sensitivity of PTAs through finding hundreds of newly discovered millisecond pulsars (MSPs[17]). Then, SKA will surely facilitate performing sky localization by using the hemisphere-averaged correlations. The other one is suppression of uncertainties of MSPs. One of the limiting factors on searching for the GWB with PTAs is the uncertainties on the solar system planetary ephemerides (e.g., M. Vallisneri et al. 2020), which are used to convert geocentric time-of-arrivals of pulses to ones measured in the solar system barycentric frame. VLBI astrometry of MSPs can suppress those uncertainties, and hence enhance the PTA sensitivities (R. Smits et al. 2011; X. Siemens et al. 2013; H. Ding et al. 2023; R. Kato & K. Takahashi 2023, and references therein).

[15] Originally, M. J. Reid & A. Brunthaler (2004) and D. Merritt et al. (2007) denoted the speed of this gravitational Brownian motion as $< V >$. Here, we denote it as $\sigma_{\rm BH/\star}$ for convenience.

[16] H. Kawai et al. (2022, 2024) suggested, on the contrary, that FDM is likely to have a smooth density distribution without such heavy FDM quasi-particles in the central region of an FDM halo. If this is the case, then the argument in this subsection may no longer hold.

[17] https://www.skao.int/en

6. Summary

In this paper, we constrain a mass of a hypothetical secondary black hole orbiting the primary SMBH in M87. To constrain q and a, we impose the following three constraints: (i) the lower limit of a, below which the SMBH binary is expected to merge; (ii) the strain amplitude of the GWB shown in the NANOGrav 15 yr data set; and (iii) a finite a_1 that can induce periodic behavior in the jet. By combining these constraints, we obtain the allowed parameter space for q and a. If either of the EAVN-detected periods (T) corresponds to the binary's orbital period, the allowed range of q is $6.9 \times 10^{-3} \leqslant q \leqslant 4.2 \times 10^{-2}$ for $T \approx 11$ yr, and $3.7 \times 10^{-2} \leqslant q \leqslant 1$ for $T \approx 0.9$ yr. VLBI astrometric monitoring of the jet base of M87 is essential to explore the allowed parameter space for q and a.

VLBI astrometric observations enable detection of sub-parsec separation SMBH binaries by tracking orbital motions, but their high cost and long duration limit target numbers. M87, with its jet periodicity, is a good candidate, particularly in the gap-window region between the NANOGrav limit and the merger limit. A 1–2 yr pilot study could reveal systematic motion, prompting longer-term observations. Challenges such as jet flares and annual parallax may be mitigated by multifrequency phase-referencing VLBI techniques. Upcoming systems, especially at 86 GHz, will improve positional accuracy and help test the SMBH binary hypothesis.

We discuss the future potential of ngVLA astrometry, expected to achieve $\sim 1\ \mu$as accuracy. While exceeding the requirements for detecting a secondary black hole in M87, this precision could investigate gravitational Brownian motion from ultralight FDM. Detecting such motion is challenging due to M87's possible secular motion in the Virgo cluster and the required sub-1 μas yr^{-1} precision, while future instruments like ngEHT and space VLBI may improve accuracy and uncover insights into FDM.

Acknowledgments

We thank the anonymous referee for providing valuable comments, which improved the paper. This work was partially supported by the MEXT/JSPS KAKENHI (JP21H01137, JP21H04488, JP22H00157, JP23H00117, and JP23K03448). H.R. is supported by the National Research Council of Science & Technology (NST)—Korea Astronomy and Space Science Institute (KASI) Postdoctoral Fellowship Program for Young Scientists at KASI in South Korea. Y.C. is supported by the Natural Science Foundation of China (grant 12303021) and the China Postdoctoral Science Foundation (grant No. 2024T170845). This work was supported by the National Research Foundation of Korea (NRF) grant funded by the Korea government (MSIT; RS-2024-00449206) and the POSCO Science Fellowship of POSCO TJ Park Foundation.

ORCID iDs

Motoki Kino https://orcid.org/0000-0002-2709-7338
Masahiro Nagashima https://orcid.org/0000-0003-2938-7096
Hyunwook Ro https://orcid.org/0000-0002-7322-6436
Yuzhu Cui https://orcid.org/0000-0001-6311-4345
Kazuhiro Hada https://orcid.org/0000-0001-6906-772X
Jongho Park https://orcid.org/0000-0001-6558-9053

References

Acciari, V. A., Aliu, E., Arlen, T., et al. 2009, Sci, 325, 444
Agazie, G., Anumarlapudi, A., Archibald, A. M., et al. 2023a, ApJL, 951, L8
Agazie, G., Anumarlapudi, A., Archibald, A. M., et al. 2023b, ApJL, 952, L37
Armitage, P. J., & Natarajan, P. 2005, ApJ, 634, 921
Bahcall, J. N., & Wolf, R. A. 1976, ApJ, 209, 214
Batcheldor, D., Robinson, A., Axon, D. J., Perlman, E. S., & Merritt, D. 2010, ApJL, 717, L6
Begelman, M. C., Blandford, R. D., & Rees, M. J. 1980, Natur, 287, 307
Blakeslee, J. P., Jordán, A., Mei, S., et al. 2009, ApJ, 694, 556
Bohn, A., Throwe, W., Hébert, F., et al. 2015, CQGra, 32, 065002
Bonetti, M., Haardt, F., Sesana, A., & Barausse, E. 2018, MNRAS, 477, 3910
Britzen, S., Fendt, C., Witzel, G., et al. 2018, MNRAS, 478, 3199
Britzen, S., Zajaček, M., Gopal-Krishna, et al. 2023, ApJ, 951, 106
Chandrasekhar, S. 1943, ApJ, 97, 255
Cheng, X., Yang, J., Zhao, G.-Y., et al. 2023, ApJL, 955, L30
Cui, Y., Hada, K., Kawashima, T., et al. 2023, Natur, 621, 711
Cunha, P. V. P., Herdeiro, C. A. R., & Rodriguez, M. J. 2018, PhRvD, 98, 044053
Dexter, J., Lutz, D., Shimizu, T. T., et al. 2020, ApJ, 905, 33
Di Cintio, P., Ciotti, L., & Nipoti, C. 2020, IAU Symp. 351, Star Clusters: From the Milky Way to the Early Universe (Cambridge: Cambridge Univ. Press), 93
Di Matteo, T., Springel, V., & Hernquist, L. 2005, Natur, 433, 604
Ding, H., Deller, A. T., Stappers, B. W., et al. 2023, MNRAS, 519, 4982
Dodson, R., Garcìa-Miró, C., Giroletti, M., et al. 2023, arXiv:2306.04516
Doeleman, S. S., Barrett, J., Blackburn, L., et al. 2023, Galax, 11, 107
D'Orazio, D. J., & Charisi, M. 2023, arXiv:2310.16896
D'Orazio, D. J., & Loeb, A. 2018, ApJ, 863, 185
El-Zant, A. A., Roupas, Z., & Silk, J. 2020, MNRAS, 499, 2575
Enoki, M., Inoue, K. T., Nagashima, M., & Sugiyama, N. 2004, ApJ, 615, 19
Enoki, M., & Nagashima, M. 2007, PThPh, 117, 241
Event Horizon Telescope Collaboration 2019a, ApJL, 875, L1
Event Horizon Telescope Collaboration 2019b, ApJL, 875, L2
Event Horizon Telescope Collaboration 2019c, ApJL, 875, L3
Event Horizon Telescope Collaboration 2019d, ApJL, 875, L4
Event Horizon Telescope Collaboration 2019e, ApJL, 875, L5
Event Horizon Telescope Collaboration 2019f, ApJL, 875, L6
Event Horizon Telescope Collaboration, Akiyama, K., Algaba, J. C., et al. 2021, ApJL, 910, L13
Event Horizon Telescope Collaboration, Akiyama, K., Alberdi, A., et al. 2024, A&A, 681, A79
Ferreira, E. G. M. 2021, A&ARv, 29, 7
Goicovic, F. G., Sesana, A., Cuadra, J., & Stasyszyn, F. 2017, MNRAS, 472, 514
Gould, A., & Rix, H.-W. 2000, ApJL, 532, L29
Gualandris, A., Read, J. I., Dehnen, W., & Bortolas, E. 2017, MNRAS, 464, 2301
Hada, K., Asada, K., Nakamura, M., & Kino, M. 2024, A&ARv, 32, 5
Hada, K., Giroletti, M., Kino, M., et al. 2014, ApJ, 788, 165
Hada, K., Kino, M., Nagai, H., et al. 2012, ApJ, 760, 52
Hellings, R. W., & Downs, G. S. 1983, ApJL, 265, L39
Hernquist, L. 1989, Natur, 340, 687
Honma, M., Tamura, Y., & Reid, M. J. 2008, PASJ, 60, 951
Hopkins, P. F., Hernquist, L., Cox, T. J., & Kereš, D. 2008, ApJS, 175, 356
Hopkins, P. F., Hernquist, L., Cox, T. J., et al. 2006, ApJS, 163, 1
Issaoun, S., Pesce, D. W., Roelofs, F., et al. 2023, Galax, 11, 28
Iwasawa, M., An, S., Matsubayashi, T., Funato, Y., & Makino, J. 2011, ApJL, 731, L9
Jenet, F. A., Hobbs, G. B., van Straten, W., et al. 2006, ApJ, 653, 1571
Jiang, W., Zhao, G.-Y., Shen, Z.-Q., et al. 2023, Galax, 11, 3
Johnson, M. D., Akiyama, K., Blackburn, L., et al. 2023, Galax, 11, 61
Johnson, M. D., Akiyama, K., Baturin, R., et al. 2024, Proc. SPIE, 13092, 130922D
Kato, R., & Takahashi, K. 2023, PhRvD, 108, 123535
Kawai, H., Kamada, A., Kamada, K., & Yoshida, N. 2024, PhRvD, 110, 023519
Kawai, H., Oguri, M., Amruth, A., Broadhurst, T., & Lim, J. 2022, ApJ, 925, 61
Kim, J.-S., Mueller, H., Nikonov, A. S., et al. 2025, A&A, 696, A169
Kocsis, B., Haiman, Z., & Menou, K. 2008, ApJ, 684, 870
Kormendy, J., & Richstone, D. 1995, ARA&A, 33, 581
Koyama, S., Kino, M., Doi, A., et al. 2015, PASJ, 67, 67
Lacey, C., & Cole, S. 1993, MNRAS, 262, 627
Lena, D., Robinson, A., Marconi, A., et al. 2014, ApJ, 795, 146

Lu, R.-S., Asada, K., Krichbaum, T. P., et al. 2023, Natur, 616, 686
Maggiore, M. 2018, Gravitational Waves: Vol. 2: Astrophysics and Cosmology (Oxford: Oxford Univ. Press)
Matsubayashi, T., Makino, J., & Ebisuzaki, T. 2007, ApJ, 656, 879
Merritt, D., Berczik, P., & Laun, F. 2007, AJ, 133, 553
Mikkola, S., & Valtonen, M. J. 1992, MNRAS, 259, 115
Milosavljević, M., & Merritt, D. 2001, ApJ, 563, 34
Milosavljević, M., & Merritt, D. 2003a, in AIP Conf. Ser. 686, The Astrophysics of Gravitational Wave Sources, ed. J. M. Centrella (Melville, NY: AIP), 201
Milosavljević, M., & Merritt, D. 2003b, in AIP Conf. Ser. 686, The Astrophysics of Gravitational Wave Sources, ed. J. M. Centrella (Melville, NY: AIP), 201
Miranda, R., Muñoz, D. J., & Lai, D. 2017, MNRAS, 466, 1170
Murphy, E. J., Bolatto, A., & Chatterjee, S. 2018, in ASP Conf. Ser. 517, Science with a Next Generation Very Large Array, ed. E. Murphy (San Francisco, CA: ASP), 3
Niinuma, K., Kino, M., Doi, A., et al. 2015, ApJL, 807, L14
Ostriker, J. P., & Hausman, M. A. 1977, ApJL, 217, L125
Peters, P. C. 1964, PhRv, 136, 1224
Quinlan, G. D. 1996, NewA, 1, 35
Rafikov, R. R. 2016, ApJ, 827, 111
Ray, M., & Hwang, C.-Y. 2024, ApJ, 974, 5
Reid, M. J., & Brunthaler, A. 2004, ApJ, 616, 872
Reid, M. J., Readhead, A. C. S., Vermeulen, R. C., & Treuhaft, R. N. 1999, ApJ, 524, 816
Ressler, S. M., Combi, L., Li, X., Ripperda, B., & Yang, H. 2024, ApJ, 967, 70
Richstone, D., Ajhar, E. A., Bender, R., et al. 1998, Natur, 385, A14
Rioja, M. J., & Dodson, R. 2020, A&ARv, 28, 6
Ro, H., Yi, K., Cui, Y., et al. 2023, Galax, 11, 33
Safarzadeh, M., Loeb, A., & Reid, M. 2019, MNRAS, 488, L90
Sasaki, T., Yamauchi, K., Yamamoto, S., & Asada, H. 2024, PhRvD, 109, 024023
Schutz, K., & Ma, C.-P. 2016, MNRAS, 459, 1737
Sesana, A., Haardt, F., Madau, P., & Volonteri, M. 2004, ApJ, 611, 623
Siemens, X., Ellis, J., Jenet, F., & Romano, J. D. 2013, CQGra, 30, 224015
Sillanpaa, A., Haarala, S., Valtonen, M. J., Sundelius, B., & Byrd, G. G. 1988, ApJ, 325, 628
Simionescu, A., Werner, N., Mantz, A., Allen, S. W., & Urban, O. 2017, MNRAS, 469, 1476
Smits, R., Tingay, S. J., Wex, N., Kramer, M., & Stappers, B. 2011, A&A, 528, A108
Su, Y., Kraft, R. P., Nulsen, P. E. J., et al. 2019, AJ, 158, 6
Sudou, H., Iguchi, S., Murata, Y., & Taniguchi, Y. 2003, Sci, 300, 1263
Tang, Y., MacFadyen, A., & Haiman, Z. 2017, MNRAS, 469, 4258
Thompson, A. R., Moran, J. M., & Swenson, G. W. J. 2001, Interferometry and Synthesis in Radio Astronomy (2nd ed.; New York: Wiley)
Vallisneri, M., Taylor, S. R., Simon, J., et al. 2020, ApJ, 893, 112
Wrobel, J. M., & Lazio, T. J. W. 2022, ApJ, 931, 12
Wyithe, J. S. B., & Loeb, A. 2003, ApJ, 590, 691
Yonemaru, N., Kumamoto, H., Kuroyanagi, S., Takahashi, K., & Silk, J. 2016, PASJ, 68, 106
Yumoto, A., Nitta, D., Chiba, T., & Sugiyama, N. 2012, PhRvD, 86, 103001
Zhao, S.-S., Jiang, W., Lu, R.-S., Huang, L., & Shen, Z. 2024, ApJ, 961, 20